

Strong-Coupling and Degeneracy Effects in Inertial Confinement Fusion Implosions

As one of the potentially viable ways to generate clean energy, inertial confinement fusion (ICF) has been pursued for decades.¹ In “hot-spot” ICF designs, a cryogenic DT capsule is driven to implode either directly by intense laser pulses² or indirectly by x rays in a hohlraum.³ At the stagnation stage, a high-density shell ($>1000\times$ solid-DT density) is assembled around the hot spot for the fusion burn to propagate, thereby generating a net energy gain. To reach such high compression, the imploding shell must stay on a low adiabat, which is conventionally characterized as α (the ratio of the fuel pressure to the Fermi-degenerate pressure). Accurate knowledge of the equation of state (EOS) of the DT fuel is essential to ICF designs¹ because the compressibility is determined by the EOS.⁴

Dynamically compressed by shocks and/or adiabatic compression waves driven by laser ablation,⁵ the imploding DT

shell undergoes a wide range of plasma conditions at densities from $\sim 0.1 \text{ g/cm}^3$ up to 1000 g/cm^3 and temperatures varying from a few electron volts to several hundred electron volts.¹ One may expect such plasmas to enter the strongly coupled and degenerate regimes, where many-body effects become important. Strongly coupled and degenerate plasma conditions are indeed accessed in low-adiabat cryogenic implosions on the OMEGA Laser System⁶ as well as at the National Ignition Facility (NIF).⁷ Examples from hydrosimulations are shown in Figs. 121.35(a)–121.35(c) for a low-adiabat ($\alpha \simeq 2.5$) cryo-DT implosion on OMEGA and in Figs. 121.35(d)–121.35(f) for a direct-drive-ignition design for the NIF. The laser pulse shapes in panels (a) and (d) are plotted. Our hydrocode simulations show that the predicted density (ρ) and temperature (T) “paths” of the driven DT shell, which are plotted in the middle panels [(b) and (e)], undergo a variety of drive stages, includ-

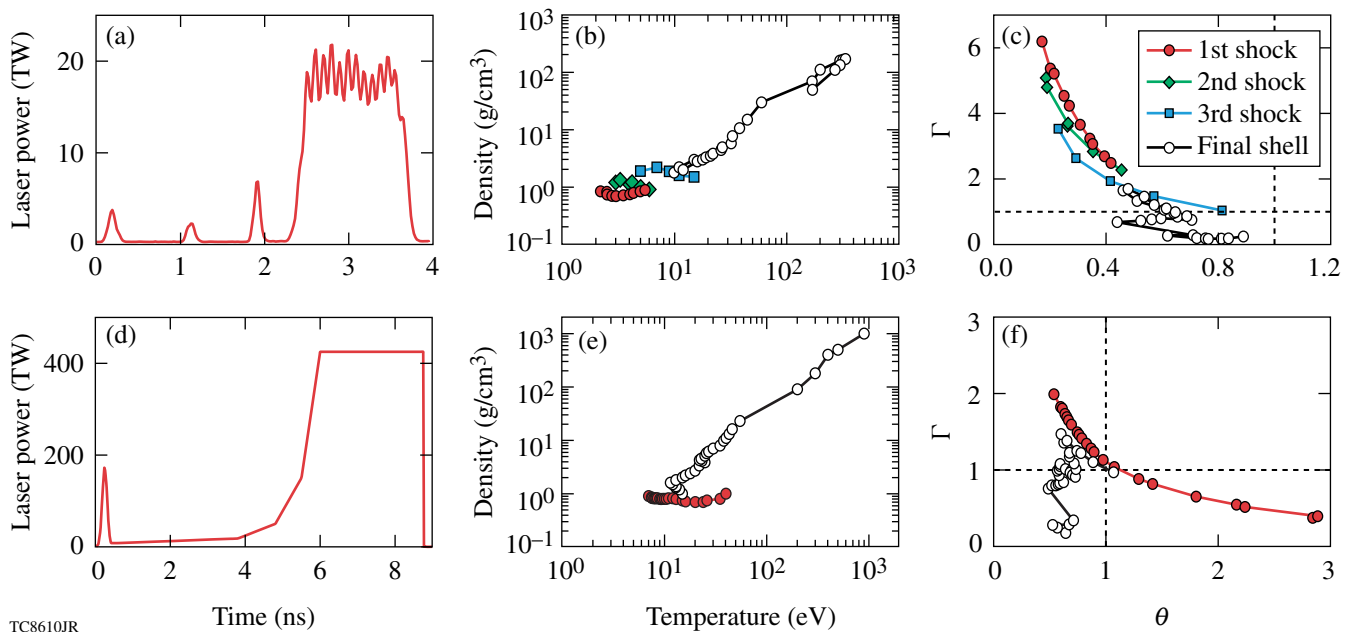


Figure 121.35

[(a)–(c)] A cryogenic-DT implosion on OMEGA; [(d)–(f)] a direct-drive-ignition design for the NIF. In both cases, strongly coupled and degenerate plasma conditions are *indeed* accessed.

ing several shocks and the final push by the main pulse. If we cast the ρ - T history of the imploding DT shell onto the plane spanned by the coupling parameter $\Gamma = 1/akT$ (where a is the Wigner–Seitz radius and k is the Boltzman constant) and the degeneracy parameter $\theta = T/T_F$ (where T_F is the Fermi temperature), we find that the imploding shell indeed undergoes the coupled ($\Gamma > 1$) and degenerate ($\theta < 1$) regimes. It is therefore expected that the effects of strong coupling and degeneracy in such plasmas would affect the compression and fusion yield in low-adiabat ICF implusions.

The effects of strong coupling and degeneracy in ICF plasmas have recently attracted much attention since they may redefine the so-called “1-D physics” of ICF implusions. For example, the essential pieces of physics models used in ICF hydrosimulations, such as the electron–ion energy relaxation rate,⁸ the thermal conductivity,⁹ and the fusion-reaction rate¹⁰ in coupled and degenerate plasmas, were recently re-examined. In recent experiments, the EOS of liquid deuterium along the principal Hugoniot around 100 to 200 GPa was measured using laser-driven shock waves,^{11–16} magnetically driven flyers,^{17,18} and convergent explosives.^{19,20} Over the years, enormous theoretical efforts have been put forth to better understand the properties of deuterium under high pressure. The widely used *SESAME* EOS table of deuterium was based on the “chemical model” of matter,^{21,22} which has adopted the liquid perturbation theory in the molecular/atomic fluid phase for ICF plasma conditions. The first-order expansion was originally used in the *SESAME* model²¹ to take only the nearest-neighbor interactions into account, which did not fully account for the effects of strong coupling and many-body degeneracy in nonideal plasmas. *Ab initio* calculations for the deuterium EOS have been performed by using the method of density functional theory–based molecular dynamics (DFT–MD)^{23–30} and the path-integral Monte Carlo (PIMC) method.^{31–35} The first-principle methods take the strong-coupling and degeneracy effects fully into account, in contrast to using chemical models.^{21,22,36–39}

For ICF applications, we are especially concerned about the EOS accuracy along the implosion path in the density–temperature plane, i.e., in the range of $\rho \sim 0.1$ to 1000 g/cm³ and $T \sim 1.0$ to 1000 eV. For these plasma conditions, the DFT-based methods become very expensive because of the large number of electronic orbitals required,⁴⁰ while the EOS can be derived efficiently with the PIMC method. This article presents a first-principles equation-of-state (FPEOS) table of deuterium from restricted PIMC calculations.⁴¹ The same method has been successfully applied to compute the deuterium EOS up to a density of $\rho = 5.388$ g/cm³ (Refs. 33 and 42) and has been

favorably compared with DFT–MD calculations.³⁴ We have used free-particle nodes to construct the many-body trial density matrix. The Coulomb interactions enter via a high- T pair-density matrix⁴³ $\rho(R, R'; \delta\beta)$. Using its convolution property, the density matrix $\rho(R, R'; \beta)$ can be expressed by

$$\rho(R, R'; \beta) = \int dR_1 dR_2 \dots dR_{M-1} \rho(R, R_1; \delta\beta) \times \rho(R_1, R_2; \delta\beta) \dots \rho(R_{M-1}, R'; \delta\beta) \quad (1)$$

with $\beta = 1/kT$ and $\delta\beta = \beta/M$, where M is the number of steps along the path in imaginary “time.” Monte Carlo methods are used to efficiently evaluate the multidimensional integration. Thermodynamic properties (associated with operator \hat{O}) of plasmas are derived from

$$\langle \hat{O} \rangle = \frac{\int dR dR' \langle R | \hat{O} | R' \rangle \langle R' | \rho(R, R'; \beta) | R \rangle}{\int dR \langle R' | \rho(R, R'; \beta) | R \rangle}. \quad (2)$$

We have performed our PIMC calculations with various numbers of atoms in periodic cubic simulation cells depending on the deuterium-density ranges: 64 atoms for $\rho < 2.5$ g/cm³, 128 atoms for $2.5 < \rho < 10.5$ g/cm³, and 256 atoms for $\rho > 10.5$ g/cm³. The time step $\delta\beta$ was chosen small enough, $1/\delta\beta \geq 75 \times kT_F$ to accurately account for interactions and degeneracy effects. Convergence tests have been done for each density range.

In Fig. 121.36(a), we compare the principal Hugoniot between our FPEOS table and the *SESAME* (5263) EOS for different temperatures marked on the curve. It is noted that this version of *SESAME* EOS is still used in ICF designs, although improvements have recently been made by Kerley.²² We have also plotted the previous Hugoniot calculated using the same PIMC method with 32 atoms and a time step of $1/\delta\beta = 8 \times 10^6$ K (Refs. 33 and 42). Good agreement is found with these previous PIMC calculations. Current PIMC simulations used 64 atoms and a smaller time step of $1/\delta\beta = 1.6 \times 10^7$ K. We found that, according to our PIMC calculations, deuterium is slightly softer than the *SESAME* prediction for pressures below ~ 2 Mbar, while it is stiffer in the pressure range of $\sim 2 < P < 100$ Mbar (the dynamic compression range in ICF). The PIMC-predicted compression of $\rho/\rho_0 \simeq 4.3$ below ~ 2 Mbar agrees better with DFT–MD calculations^{26,28} and EOS measurements using magnetically driven flyers.^{17,18} It may also agree with the laser-shock results^{15,16} after the quartz standard used in experiments is corrected.⁴⁴ To give an interpretation of these discrepancies, in Figs. 121.36(b) and 121.36(c) we have plotted the percentage differences in pressure and energy versus

density, for two temperatures $T = 344.47$ eV and $T = 21.54$ eV. The statistical error bars of our PIMC results are also marked. At $T = 344.47$ eV, both the pressure and energy from PIMC and *SESAME* are within $\sim 1\%$. This is expected because plasmas at such high temperatures are classical ($\Gamma \ll 1$, $\theta \gg 1$), where both PIMC and *SESAME* should agree. The PIMC and *SESAME* Hugoniot curves above 344 eV are identical, as shown in

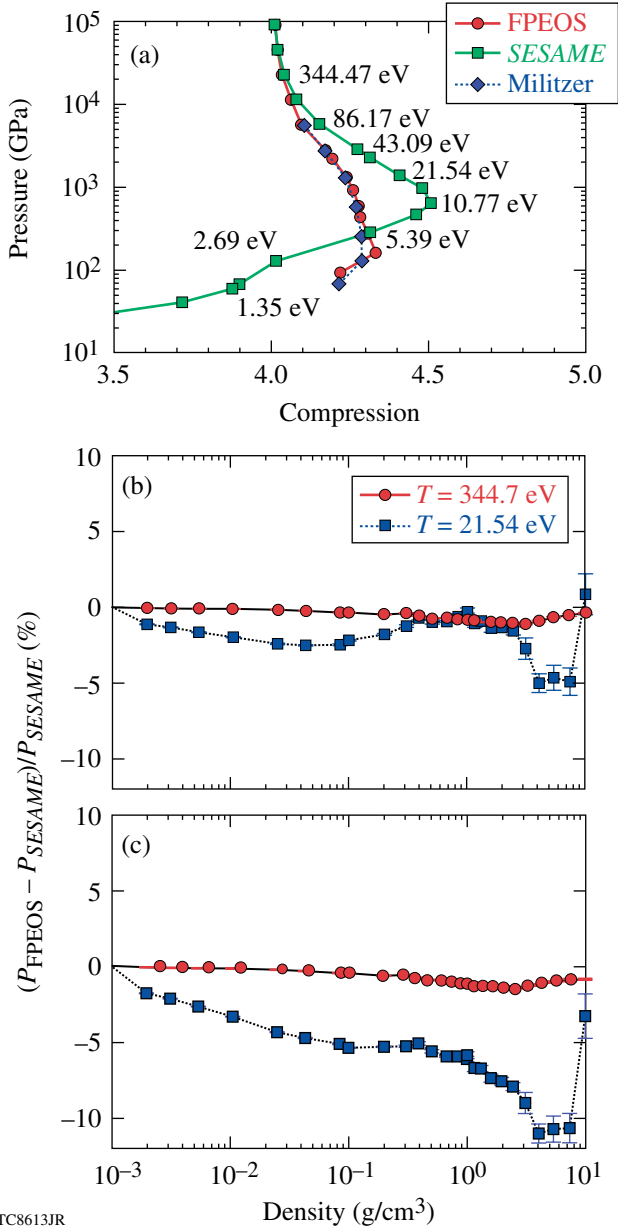
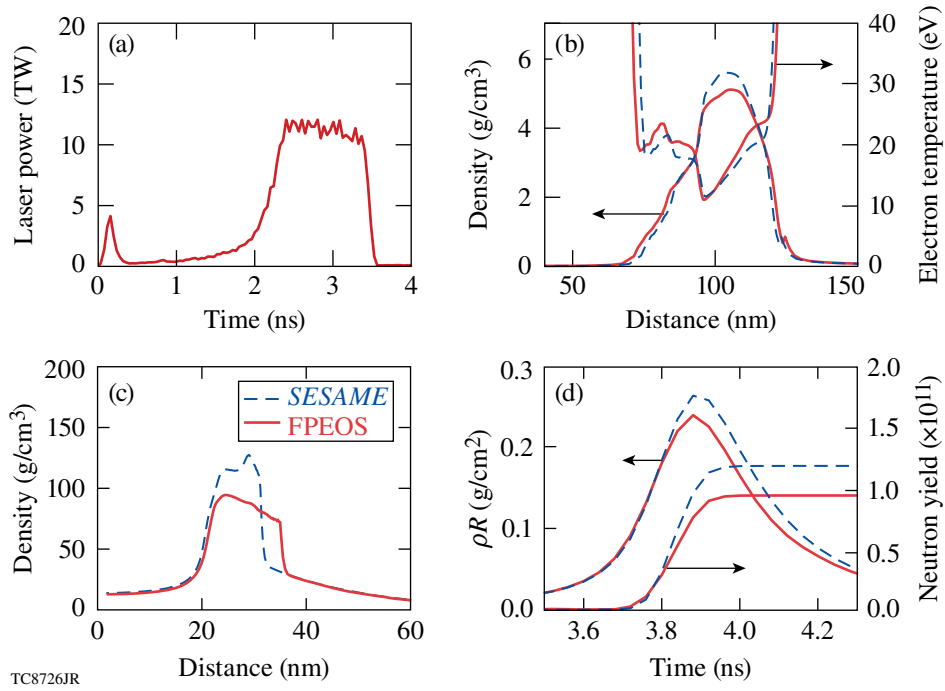


Figure 121.36 (a) The principal Hugoniot for liquid deuterium. The relative deviation in (b) pressure and (c) energy between the FPEOS and *SESAME* as a function of density, for temperatures $T = 344.7$ eV (red circles) and $T = 21.54$ eV (blue squares).

Fig. 121.36(a). For a lower temperature of 21.54 eV, however, the energy difference is larger, as indicated in Fig. 121.36(c). For the principal Hugoniot, in the density range of $\rho = 0.6$ to 0.8 g/cm^3 , the internal energy in FPEOS is $\sim 6\%$ lower than that of *SESAME* (for this comparison, the zero energy has been set to the ground state of an isolated molecule, $E_0 = -15.886$ eV), even though the pressure is comparable in both within $\sim 1\%$. According to the Hugoniot equation [$E_f - E_0 + (1/2)(P_f + P_0) \times (V_f - V_0) = 0$], the final state can be expressed as $E_f + (1/2) \times P_f V_f \simeq E_0 + (1/2) P_f V_0$ because of $P_f \gg P_0$, where (P_0, E_0, V_0) and (P_f, E_f, V_f) are the initial and final pressure, energy, and volume of deuterium. Therefore, with the similar value of P_f , the smaller E_f predicted by the FPEOS requires larger V_f to satisfy the Hugoniot equation.⁴⁵ Larger V_f relative to the *SESAME* case means a smaller final density and compression, as seen in Fig. 121.36(a). Such discrepancy was noticed by Kerley²² in 2003; with some improvements to the ionization equilibrium model adopted in *SESAME*, he succeeded in decreasing the *SESAME* compression to better agree with the first-principle calculations in this high-pressure (~ 10 -Mbar) regime.²² The lower internal energy in FPEOS, for $T < 100$ eV, is attributed to many-body interactions. Figure 121.36(c) indicates that as the density increases, the relative deviation in energy reaches a maximum of $\sim 11\%$ around $\rho \sim 4$ to 5 g/cm^3 ($\Gamma \simeq 1.3$ and $\theta \simeq 0.4$) for this isothermal curve at $T = 21.54$ eV. The *SESAME* model again agrees with PIMC calculations at very high densities (e.g., $\rho = 10$ g/cm^3), as local screening was correctly accounted for in chemical models.^{21,22}

From PIMC calculations, we have derived a first-principles EOS table for deuterium, which covers the typical ICF fuel conditions of $\rho = 0.002$ to 1596 g/cm^3 and $T = 1.35$ eV to 5.5 keV. For each density point, we have performed PIMC calculations including low temperature corresponding to $\theta = T/T_F \simeq 0.1$. To comply with the *SESAME* format used in our hydrocodes, we have added the experimentally benchmarked low- T (< 1.35 -eV) *SESAME* points to our FPEOS table, although those points are not actually used in ICF hydrocodes (except for defining the initial state). The high-temperature limit of $T > 5.5$ keV is obtained by linearly extrapolating (in T) the highest PIMC point since ideal plasma conditions are expected at high temperatures.

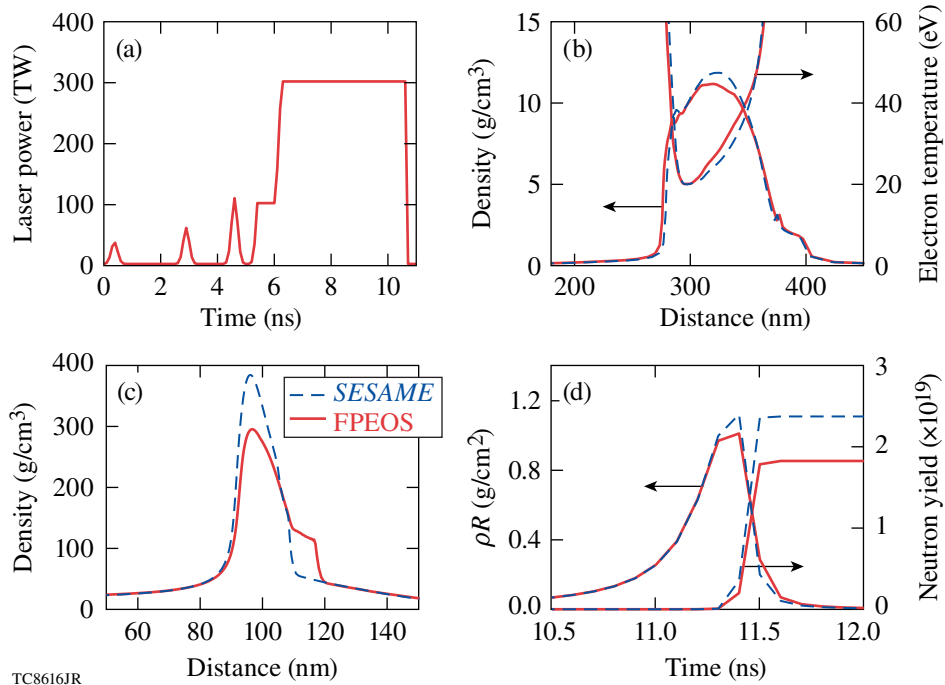
With our FPEOS table, we can now explore the implications of strong-coupling and degeneracy effects in ICF implosions using hydrocodes. Results are shown in Figs. 121.37 and 121.38, respectively, for a cryogenic D_2 implosion ($\alpha \simeq 2.5$) on the OMEGA Laser System and a direct-drive DT design on the NIF. We have used the 1-D radiative hydrocode *LILAC*⁴⁶ to



TC8726JR

Figure 121.37

The hydrocode simulations of a cryogenic D₂ implosion on OMEGA using the FPEOS table (solid red line) and the *SESAME* EOS table (dashed blue line): (a) the laser pulse shape; (b) the density and temperature profiles of the imploding D₂ shell at the end of laser pulse ($t = 3.6$ ns); (c) the density profile at peak compression; and (d) the areal density (ρR) and neutron yield as functions of time.



TC8616JR

Figure 121.38

Similar to Fig. 121.37 but for a NIF direct-drive-ignition design.

perform these simulations. In Fig. 121.37(a), we plot the pulse shape used to implode a cryogenic D_2 target (877- μm diameter) with a 10- μm CD ablator and 95 μm of D_2 ice. Figure 121.37(b) shows the density and temperature profiles at the end of the laser pulse ($t = 3.6$ ns) from both the FPEOS and *SESAME* simulations. The shell's peak density and average temperature were $\rho_p \sim 5 \text{ g/cm}^3$ and $T \sim 15 \text{ eV}$, which correspond to the strongly coupled and degenerate regime with $\Gamma \simeq 1.7$ and $\theta \simeq 0.3$. It is shown that the FPEOS simulation predicted $\sim 10\%$ -lower ρ_p but higher temperature relative to the *SESAME* prediction. As the Hugoniot comparison indicated in Fig. 121.36(a), the FPEOS is slightly stiffer than *SESAME* in this temperature range, which explains the lower ρ_p . The slightly higher temperature in the FPEOS case originated from the lower internal energy [see Fig. 121.36(c)]. Since the laser ablation does the work/energy to the shell compression and its kinetic motion, a lower internal energy in FPEOS means more energy is partitioned to heat the shell, thereby resulting in a slightly higher temperature. Such a temperature increase and density drop can have consequences in the implosion performance. At the stagnation stage (peak compression), Fig. 121.37(c) shows that the peak density is $\sim 30\%$ lower according to FPEOS ($\rho_p \simeq 90 \text{ g/cm}^3$) compared to *SESAME* ($\rho_p \simeq 130 \text{ g/cm}^3$). The peak areal density $(\rho R)_{\text{peak}}$ and neutron yield were also reduced by $\sim 10\%$ to 20% as shown in Fig. 121.37(d). The neutron-averaged areal density $\langle \rho R \rangle_n$ predicted with FPEOS was $\sim 198 \text{ mg/cm}^2$, which is in better agreement with the experimental measured $\langle \rho R \rangle_n = 202 \pm 7 \text{ mg/cm}^2$ (Ref. 47), in contrast to the *SESAME* prediction of $\langle \rho R \rangle_n = 247 \text{ mg/cm}^2$. Nonuniformities cannot account for the large discrepancy between measurements and *SESAME* predictions, as we have noted that certain perturbations in experiments can reduce the neutron yield⁴⁸ but hardly affect the compression ρR .

A similar effect was seen for the NIF designs. Figure 121.38 shows an example for a NIF target ($\phi = 3.37 \text{ mm}$) having a 37- μm CH ablator and 150 μm of DT ice. At the end of the laser pulse [$t = 10.7$ ns in Fig. 121.38(b)], we also found a decrease in ρ_p and a temperature increase for the FPEOS relative to *SESAME* simulations. The peak density near the stagnation dropped from $\rho_p = 383 \text{ g/cm}^3$ (*SESAME*) to $\rho_p = 294 \text{ g/cm}^3$ (FPEOS), as is indicated by Fig. 121.38(c). The resulting ρR and neutron yield as a function of time are plotted in Fig. 121.38(d). The peak ρR dropped from 1.1 g/cm^2 (*SESAME*) to 1.0 g/cm^2 (FPEOS), while the yield dropped from the *SESAME*-predicted value of $Y = 2.4 \times 10^{19}$ to 1.8×10^{19} for the FPEOS simulation. Consequently, the energy gain dramatically decreased from 45 (*SESAME*) to 34 (FPEOS).

In summary, we have derived a first-principles equation-of-state table of deuterium for ICF applications from PIMC calculations. The FPEOS table covers the typical fuel density and temperature conditions in ICF implosions. In comparison with the *SESAME* table, the FPEOS predicts $\sim 10\%$ -lower internal energy but comparable pressure (within few percent) for strongly coupled and degenerate plasma conditions. Hydrosimulations using the FPEOS table indicate significant decreases in the predicted peak density ($\sim 30\%$ to 40%). The results also show a reduction in the peak areal density ρR ($\sim 10\%$) and the neutron yield (energy gain) by $\sim 20\%$ with respect to the corresponding *SESAME* simulations. The compression (ρR) predicted from FPEOS agrees better with experiments. The FPEOS table will become more important for even lower adiabat ($\alpha \simeq 1$ to 2) ICF target designs since one expects strong coupling and degeneracy effects to increase in such plasmas.

ACKNOWLEDGMENT

This work was supported by U.S. Department of Energy Office of Inertial Confinement Fusion under Cooperative Agreement No. DE-FC52-08NA28302, the University of Rochester, and New York State Energy Research and Development Authority. S. X. Hu thanks the National Science Foundation for its support under the NSF-TeraGrid grant PHY090093. A portion of this research was carried out on the NICS' Kraken Supercomputer. B. Militzer acknowledges support from UC's laboratory research program, NSF, and NASA.

REFERENCES

1. S. Atzeni and J. Meyer-ter-Vehn, *The Physics of Inertial Fusion: Beam Plasma Interaction, Hydrodynamics, Hot Dense Matter*, International Series of Monographs on Physics (Clarendon Press, Oxford, 2004).
2. R. L. McCrory, D. D. Meyerhofer, R. Betti, R. S. Craxton, J. A. Delettrez, D. H. Edgell, V. Yu Glebov, V. N. Goncharov, D. R. Harding, D. W. Jacobs-Perkins, J. P. Knauer, F. J. Marshall, P. W. McKenty, P. B. Radha, S. P. Regan, T. C. Sangster, W. Seka, R. W. Short, S. Skupsky, V. A. Smalyuk, J. M. Soares, C. Stoeckl, B. Yaakobi, D. Shvarts, J. A. Frenje, C. K. Li, R. D. Petrasso, and F. H. Séguin, *Phys. Plasmas* **15**, 055503 (2008).
3. J. D. Lindl, *Phys. Plasmas* **2**, 3933 (1995).
4. S. X. Hu, V. A. Smalyuk, V. N. Goncharov, J. P. Knauer, P. B. Radha, I. V. Igumenshchev, J. A. Marozas, C. Stoeckl, B. Yaakobi, D. Shvarts, T. C. Sangster, P. W. McKenty, D. D. Meyerhofer, S. Skupsky, and R. L. McCrory, *Phys. Rev. Lett.* **100**, 185003 (2008).
5. S. X. Hu, V. A. Smalyuk, V. N. Goncharov, S. Skupsky, T. C. Sangster, D. D. Meyerhofer, and D. Shvarts, *Phys. Rev. Lett.* **101**, 055002 (2008).
6. T. R. Boehly, D. L. Brown, R. S. Craxton, R. L. Keck, J. P. Knauer, J. H. Kelly, T. J. Kessler, S. A. Kumpan, S. J. Loucks, S. A. Letzring, F. J. Marshall, R. L. McCrory, S. F. B. Morse, W. Seka, J. M. Soares, and C. P. Verdon, *Opt. Commun.* **133**, 495 (1997).

7. J. Paisner *et al.*, *Laser Focus World* **30**, 75 (1994).
8. M. S. Murillo and M. W. C. Dharma-wardana, *Phys. Rev. Lett.* **100**, 205005 (2008); M. W. C. Dharma-wardana, *Phys. Rev. Lett.* **101**, 035002 (2008); B. Jeon *et al.*, *Phys. Rev. E* **78**, 036403 (2008); G. Dimonte and J. Daligault, *Phys. Rev. Lett.* **101**, 135001 (2008); J. N. Glosli *et al.*, *Phys. Rev. E* **78**, 025401 (R) (2008); L. X. Benedict *et al.*, *Phys. Rev. Lett.* **102**, 205004 (2009).
9. V. Recoules *et al.*, *Phys. Rev. Lett.* **102**, 075002 (2009).
10. E. L. Pollock and B. Militzer, *Phys. Rev. Lett.* **92**, 021101 (2004).
11. L. B. Da Silva *et al.*, *Phys. Rev. Lett.* **78**, 483 (1997).
12. G. W. Collins *et al.*, *Science* **281**, 1178 (1998).
13. G. W. Collins *et al.*, *Phys. Plasmas* **5**, 1864 (1998).
14. A. N. Mostovych *et al.*, *Phys. Rev. Lett.* **85**, 3870 (2000); A. N. Mostovych *et al.*, *Phys. Plasmas* **8**, 2281 (2001).
15. T. R. Boehly, D. G. Hicks, P. M. Celliers, T. J. B. Collins, R. Earley, J. H. Eggert, D. Jacobs-Perkins, S. J. Moon, E. Vianello, D. D. Meyerhofer, and G. W. Collins, *Phys. Plasmas* **11**, L49 (2004).
16. D. G. Hicks, T. R. Boehly, P. M. Celliers, J. H. Eggert, S. J. Moon, D. D. Meyerhofer, and G. W. Collins, *Phys. Rev. B* **79**, 014112 (2009).
17. M. D. Knudson *et al.*, *Phys. Rev. Lett.* **87**, 225501 (2001); M. D. Knudson *et al.*, *Phys. Rev. Lett.* **90**, 035505 (2003).
18. M. D. Knudson *et al.*, *Phys. Rev. B* **69**, 144209 (2004).
19. S. I. Belov *et al.*, *JETP Lett.* **76**, 433 (2002).
20. V. E. Fortov *et al.*, *Phys. Rev. Lett.* **99**, 185001 (2007).
21. G. I. Kerley, *Phys. Earth Planet. Inter.* **6**, 78 (1972).
22. G. I. Kerley, Sandia National Laboratory, Albuquerque, NM, Report SAND2003-3613 (2003).
23. L. Collins *et al.*, *Phys. Rev. E* **52**, 6202 (1995).
24. T. J. Lenosky *et al.*, *Phys. Rev. B* **61**, 1 (2000).
25. G. Galli *et al.*, *Phys. Rev. B* **61**, 909 (2000).
26. L. A. Collins *et al.*, *Phys. Rev. B* **63**, 184110 (2001).
27. J. Cl rouin and J.-F. Dufr che, *Phys. Rev. E* **64**, 066406 (2001).
28. M. P. Desjarlais, *Phys. Rev. B* **68**, 064204 (2003).
29. S. A. Bonev, B. Militzer, and G. Galli, *Phys. Rev. B* **69**, 014101 (2004).
30. S. A. Bonev *et al.*, *Nature* **431**, 669 (2004).
31. C. Pierleoni *et al.*, *Phys. Rev. Lett.* **73**, 2145 (1994).
32. W. R. Magro *et al.*, *Phys. Rev. Lett.* **76**, 1240 (1996).
33. B. Militzer and D. M. Ceperley, *Phys. Rev. Lett.* **85**, 1890 (2000).
34. B. Militzer *et al.*, *Phys. Rev. Lett.* **87**, 275502 (2001).
35. V. Bezkrvniy *et al.*, *Phys. Rev. E* **70**, 057401 (2004); V. S. Filinov *et al.*, *Plasma Phys. Rep.* **31**, 700 (2005).
36. D. Saumon and G. Chabrier, *Phys. Rev. A* **46**, 2084 (1992).
37. M. Ross, *Phys. Rev. B* **58**, 669 (1998).
38. F. J. Rogers, *Contrib. Plasma Phys.* **41**, 179 (2001).
39. H. Juranek, R. Redmer, and Y. Rosenfeld, *J. Chem. Phys.* **117**, 1768 (2002).
40. L. A. Collins, Los Alamos National Laboratory, private communication (2009).
41. D. M. Ceperley, *Rev. Mod. Phys.* **67**, 279 (1995).
42. B. Militzer, "Path Integral Monte Carlo Simulations of Hot Dense Hydrogen," Ph.D. thesis, University of Illinois at Urbana-Champaign, 2000.
43. B. Militzer, "Computation of the High Temperature Coulomb Density Matrix in Periodic Boundary Conditions," to be published in *Physical Review E*.
44. M. D. Knudson and M. P. Desjarlais, *Phys. Rev. Lett.* **103**, 225501 (2009).
45. B. Militzer, *Phys. Rev. Lett.* **97**, 175501 (2006).
46. J. Delettrez, R. Epstein, M. C. Richardson, P. A. Jaanimagi, and B. L. Henke, *Phys. Rev. A* **36**, 3926 (1987).
47. T. C. Sangster, V. N. Goncharov, P. B. Radha, V. A. Smalyuk, R. Betti, R. S. Craxton, J. A. Delettrez, D. H. Edgell, V. Yu. Glebov, D. R. Harding, D. Jacobs-Perkins, J. P. Knauer, F. J. Marshall, R. L. McCrory, P. W. McKenty, D. D. Meyerhofer, S. P. Regan, W. Seka, R. W. Short, S. Skupsky, J. M. Soures, C. Stoeckl, B. Yaakobi, D. Shvarts, J. A. Frenje, C. K. Li, R. D. Petrasso, and F. H. S guin, *Phys. Rev. Lett.* **100**, 185006 (2008).
48. S. X. Hu, P. B. Radha, J. A. Marozas, R. Betti, T. J. B. Collins, R. S. Craxton, J. A. Delettrez, D. H. Edgell, R. Epstein, V. N. Goncharov, I. V. Igumenshchev, F. J. Marshall, R. L. McCrory, D. D. Meyerhofer, S. P. Regan, T. C. Sangster, S. Skupsky, V. A. Smalyuk, Y. Elbaz, and D. Shvarts, *Phys. Plasmas* **16**, 112706 (2009).